MITSUBISHI ELECTRIC RESEARCH LABORATORIES
http://www.merl.com

Application of coupled mode theory on radiative heat transfer between layered Lorentz materials

Lin, C.; Wang, B.; Teo, K.H.

TR2017-069 May 2017

Abstract

Coupled mode theory (CMT) provides a simple and clear framework to analyze the radiation energy exchange between reservoirs. We apply CMT to analyze the radiative heat transfer between layered Lorentz materials, whose dielectric functions can be approximated by the Lorentz oscillator model. By comparing the transmissivity computed by the exact solution to that computed by CMT, we find CMT generally gives a good approximation for this class of materials. The biggest advantage of CMT analysis, in our opinion, is that only the (complex) resonant energies are needed to obtain the radiation energy transfer; the knowledge of spatial profile of resonances is not required. Several issues, including how to choose the resonant modes, what these modes represent, and the limitation of this method, are discussed. Finally, we also apply CMT method to the electronic systems, demonstrating the generality of this formalism.

Journal of Applied Physics

Application of coupled mode theory on radiative heat transfer between layered Lorentz materials

Chungwei Lin, Bingnan Wang, and Koon Hoo Teo
Mitsubishi Electric Research Laboratories
201 Broadway, Cambridge, MA 02139, USA
(Dated: April 17, 2017)

Coupled mode theory (CMT) provides a simple and clear framework to analyze the radiation energy exchange between reservoirs. We apply CMT to analyze the radiative heat transfer between layered Lorentz materials, whose dielectric functions can be approximated by the Lorentz oscillator model. By comparing the transmissivity computed by the exact solution to that computed by CMT, we find CMT generally gives a good approximation for this class of materials. The biggest advantage of CMT analysis, in our opinion, is that only the (complex) resonant energies are needed to obtain the radiation energy transfer; the knowledge of spatial profile of resonances is not required. Several issues, including how to choose the resonant modes, what these modes represent, and the limitation of this method, are discussed. Finally, we also apply CMT method to the electronic systems, demonstrating the generality of this formalism.

PACS numbers:

I. INTRODUCTION

Coupled mode theory (CMT) is a phenomenological but powerful tool to describe a system whose behavior is governed by a few resonant modes [1], including photonic devices [2–4] and wireless power transfer systems [5, 6]. CMT has recently been used to study the radiation energy transfer [7, 8], and is shown to greatly reduce the computational expenses while maintaining the sufficient accuracy. The near-field thermophotovoltaic (TPV) system [9–18], which converts heat to the electricity by reshaping the radiation spectrum, is another system where CMT analysis naturally applies. Traditionally, the radiative heat transfer between the heat reservoirs (such as the emitter and the PV cell in a TPV system) is analyzed using dyadic Green function [13, 19–22] and the fluctuation-dissipation theorem [23]. The method is exact, but the resulting expression is complicated and is not easy to analyze. Recently, Karalis and Joannopoulos developed a CMT framework that can describe the radiative heat exchange between reservoirs, and applied it the metal/dielectric interface [24]. Their CMT-based formalism not only describes all possible loss mechanisms, but also gives a unified scheme, via introducing the "generalized Planck distribution" [25, 26], to compute both the radiation input power and the resulting electric output power. Based on CMT, they are able to include general decaying mechanisms, and design system configurations that achieve the high heat-to-electricity efficiency [27]. In this work, we apply CMT framework to analyze another class of materials, whose dielectric functions can be approximated by the Lorentz oscillator model. Generally, a material that has a dipolar coupling to the electric field displays the Lorentzian profile in the dielectric function, and in this paper we refer these materials as "Lorentz material". The origin of the dipolar coupling can come from optical phonons [28, 29], valance-to-conduction band transition [30], or the quantum states of nano-size particles [31]. We are particular interested in the heat transfer between a material of Lorentzian dielectric function and another material whose dielectric function is characterized by the interband transitions. By comparing the transmissivity computed using exact solution to that using CMT, we find that CMT generally gives satisfactory results for this class of materials. In our opinion, the biggest advantage of CMT analysis is that only the (complex) resonant energies are needed to obtain a good approximation of radiation energy transfer; the information of spatial profile of resonances is not required. The knowledge of resonant energies can be from some numerical solver or experiments. However, CMT analysis is *not* numerically useful for systems not supporting any resonances, and thus do not provide a quantitative description on some interesting classes of systems, such as the micro-gap TPV [32, 33] and meta-materials supporting continuous hyperbolic modes [34]. Several issues, including how to choose the resonant modes, what these resonant modes represent, the limitation of the method, and its generalization to electronic systems are discussed.

The rest of the paper is organized as follows. In Section II, we review how CMT is used to describe the radiation energy transfer between reservoirs fixed at different temperatures. In Section III, we study several examples involving the Lorentz oscillator model of dielectric functions. Different choices of resonant modes are compared and discussed. In Section IV, we apply the CMT method to the one-dimensional (1D) electronic system. The limitation of CMT as a numerical solver is discussed in this system. A brief summary is given in Section V. In the Appendix, we give a short derivation on the eigenmodes of planar structures.

II. REVIEW OF COUPLED MODE THEORY ON RADIATIVE HEAT TRANSFER

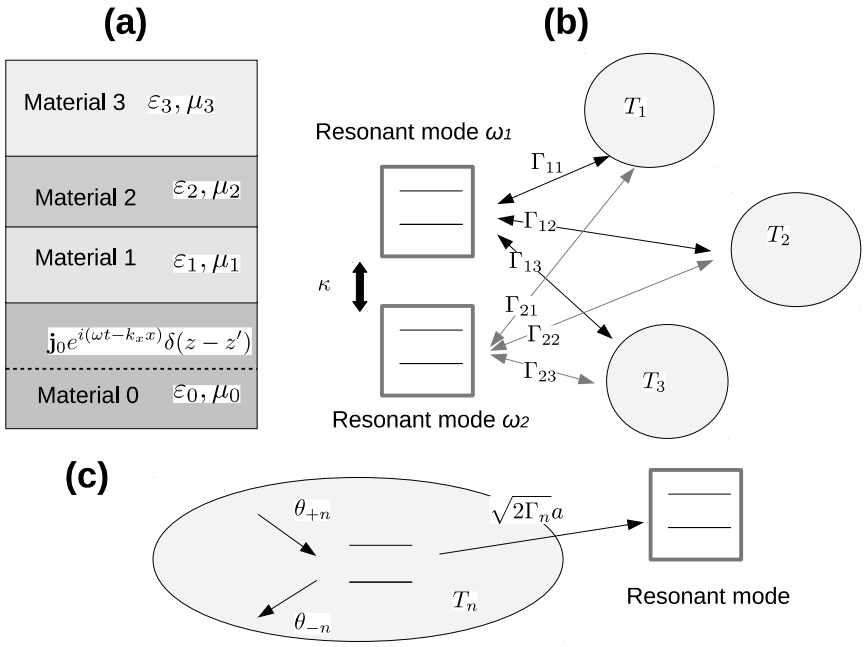

FIG. 1: (a) The "first-principle" description of the radiative heat transfer. Thermal electric currents, whose amplitudes depends on the temperature, radiate EM wave from one reservoir to other reservoirs. Summing over all contributions gives the net radiative heat transfer. (b) The CMT description of the radiative heat transfer. The key ingredient of CMT is how (cavity) modes of different reservoirs couple. The couplings between cavity modes of different reservoirs are not direct, but originate their (effective) coupling to common resonant modes. (c) The coupling between the reservoir cavity mode and the resonance is from their coupling to a common loss object (e.g. a two-level atom). Inside nth reservoir specified by T_n, the nth loss object receives the photons from (the cavity mode of) the nth reservoir, and emits photons to both nth reservoir and the resonant mode.

A. Radiation heat transfer

Microscopically, the heat transfer via radiation is illustrated in Fig. 1(a). The thermal energy generates some random electric current density, whose temperature-dependent amplitude is governed by the fluctuation-dissipation theorem [23]. These random thermal currents radiate electromagnetic (EM) fields which satisfy boundary conditions imposed by Maxwell's equations. By evaluating the Poynting vector using dyadic Green's function [20–22], one can determine the thermal radiation power from first principle. For the planar structure, where the in-plane momentum $\mathbf{K}$ (defines $x-y$ plane) is a good quantum number, the Poynting vector normal to the plane as a function z has the form

$$\begin{aligned} S_z(z) &= \int_0^\infty \frac{d\omega}{2\pi}\hbar\omega\left[\Theta_i(\omega)-\Theta_j(\omega)\right]\frac{A}{(2\pi)^2}\int d^2\mathbf{K}\varepsilon(\omega,\mathbf{K};z) \\ &= \int_0^\infty \frac{d\omega}{2\pi}\hbar\omega\left[\Theta_i(\omega)-\Theta_j(\omega)\right]\frac{A(2\pi)}{(2\pi)^2}\int k\,dk\,\varepsilon(\omega,k;z) \end{aligned} \tag{1}$$

Here $\Theta_i(\omega) = \left[e^{\hbar\omega/(k_B T_i)}-1\right]^{-1}$ is the Planck distribution, k_B is the Boltzmann constant, $k = |\mathbf{K}|$, and $\varepsilon(\omega, k; z)$, which is dimensionless and will be related to the transmissivity, is a function determined by the spatial configuration. We refer Eq. (1) as the exact solution, and the detailed expression can be found in several references [20–22]. Note that when $\Theta_i(\omega)$ is replaced by the "generalized Planck distribution" [25, 26], one is able to describe the reservoir maintained at a nonzero voltage [24]. The generalization is straightforward, and we do not consider this situation in this work.

B. Coupled mode theory

We now briefly review the coupled mode theory (CMT) applied to the radiative heat transfer, developed by Karalis and Joannopoulos in Ref. [24]. With CMT, the (complex) resonant energies are all we need in order to compute the energy exchange via thermal radiation; the spatial profiles of EM fields are not required. It is particularly useful when the whole system sustains only a few resonant modes within the energy window of interest.

The thermal radiative energy of a given reservoir is governed by the cavity-mode occupation number of that reservoir. The radiative energy transfer between reservoirs concerns the steady-state cavity-mode occupation numbers of all reservoirs, which can be different from their respective equilibrium values when there are couplings between these cavity modes. The key ingredient of CMT is to model how cavity modes from different reservoirs couple to one another, and the whole CMT framework is illustrated in Fig. 1(b) and (c). The couplings between cavity modes of different reservoirs are not direct, but originate their (effective) coupling to common resonant modes [Fig. 1(b)]. Furthermore, the coupling between the cavity mode (of one reservoir) and the resonant mode is also not direct, but originates their (direct) coupling to the common "loss objects" (or "loss mechanism") residing in that reservoir [Fig. 1(c)]. An example of loss objects is two-level atoms, which absorb and emit photons of a certain energy; the photons can be from reservoir cavity mode and/or the resonant modes.

We now make the above description more quantitative. Here we consider two resonant modes of resonant frequencies ω_1 and ω_2, specified by amplitudes a_1 and a_2. The coupling between the two resonant modes is κ. Each resonance also couples to "loss objects" residing inside reservoirs. The equation of motion for these two modes are

$$\begin{aligned}
\frac{d}{dt}a_1(t) &= (-i\omega_1 - \sum_n \Gamma_{1n})a_1(t) + i\kappa a_2 + \sum_n \sqrt{2\Gamma_{1n}}\theta_{+1n}, \\
\theta_{-1n} &= \theta_{+1n} - \sqrt{2\Gamma_{1n}}a_1, \\
\frac{d}{dt}a_2(t) &= (-i\omega_2 - \sum_n \Gamma_{2n})a_2(t) + i\kappa a_1 + \sum_n \sqrt{2\Gamma_{2n}}\theta_{+2n}, \\
\theta_{-2n} &= \theta_{+2n} - \sqrt{2\Gamma_{2n}}a_2.
\end{aligned} \tag{2}$$

In Eq. (2), Γ_{1n} (Γ_{2n}) represents the coupling between the resonant mode 1 (2) and the loss object $1n$ ($2n$). $\langle\theta^*_{+1n}\theta_{+1n}\rangle = \Theta_{1n}(\omega)$ is the mean number of ω-photons injected by the nth reservoir (i.e. the cavity-mode photon of nth reservoir) at T_n into the loss object $1n$; $\langle\theta^*_{-1n}\theta_{-1n}\rangle$ is the mean number of ω-photons reflected from the loss object $1n$ back to the nth reservoir [8, 24]. The second and fourth lines of Eq. (2) correspond to the flux conservation, and are illustrated in Fig. 1(c) [35].

The steady-state solution at frequency ω, by denoting $\delta_i = \omega - \omega_i + i\sum_n \Gamma_{in}$, is

$$\begin{aligned}
a_1 &= i\frac{\sum_n \sqrt{2\Gamma_{1n}}\theta_{+1n} - \kappa\sum_n \sqrt{2\Gamma_{2n}}\theta_{+2n}}{\delta_1\delta_2 - \kappa^2}, \\
\langle|a_1|^2\rangle &= \frac{|\delta_2|^2\sum_n 2\Gamma_{1n}\langle|\theta_{+1n}|^2\rangle - \kappa^2\sum_n 2\Gamma_{2n}\langle|\theta_{+2n}|^2\rangle}{|\delta_1\delta_2 - \kappa^2|^2}.
\end{aligned} \tag{3}$$

Interchanging $1 \leftrightarrow 2$ gives a_2 and $\langle|a_2|^2\rangle$. The net number of photons emitted by loss object $1i$ and $2i$ are

$$\begin{aligned}
N_{1i}(\omega) &= \langle|\theta_{+1i}|^2\rangle - \langle|\theta_{-1i}|^2\rangle \\
&= \sum_{j(j\neq i)} [\Theta_{1i}(\omega) - \Theta_{1j}(\omega)] \frac{4\Gamma_{1i}\Gamma_{1j}|\delta_2|^2}{|\delta_1\delta_2 - \kappa^2|^2} + \sum_j [\Theta_{1i}(\omega) - \Theta_{2j}(\omega)] \frac{4\Gamma_{1i}\Gamma_{2j}|\kappa|^2}{|\delta_1\delta_2 - \kappa^2|^2} \\
N_{2i}(\omega) &= \langle|\theta_{+2i}|^2\rangle - \langle|\theta_{-2i}|^2\rangle \\
&= \sum_{j(j\neq i)} [\Theta_{2i}(\omega) - \Theta_{2j}(\omega)] \frac{4\Gamma_{2i}\Gamma_{2j}|\delta_1|^2}{|\delta_1\delta_2 - \kappa^2|^2} + \sum_j [\Theta_{2i}(\omega) - \Theta_{1j}(\omega)] \frac{4\Gamma_{2i}\Gamma_{1j}|\kappa|^2}{|\delta_1\delta_2 - \kappa^2|^2}
\end{aligned} \tag{4}$$

Based on Eq. (4), one can define the transmissivity of the radiation energy transfer from ith to jth reservoir [24].

There are four classes of transmissivity describing the radiation energy transfer from loss mechanism a to b:

$$\begin{aligned}
\varepsilon_{1i,1j} &= \frac{4\Gamma_{1i}\Gamma_{1j}|\delta_2|^2}{|\delta_1\delta_2-\kappa^2|^2}, \\
\varepsilon_{1i,2j} &= \frac{4\Gamma_{1i}\Gamma_{2j}|\kappa|^2}{|\delta_1\delta_2-\kappa^2|^2} \\
\varepsilon_{2i,1j} &= \frac{4\Gamma_{2i}\Gamma_{1j}|\delta_1|^2}{|\delta_1\delta_2-\kappa^2|^2}, \\
\varepsilon_{2i,2j} &= \frac{4\Gamma_{2i}\Gamma_{2j}|\kappa|^2}{|\delta_1\delta_2-\kappa^2|^2}
\end{aligned} \tag{5}$$

The photon transfer rate between loss mechanisms a and b, at a given frequency ω, is simply the transimissivity multiplied by the difference of Planck distributions. For example, the net photon transfer rate between $1i$ and $1j$ at energy $\hbar\omega$ is $\varepsilon_{1i,1j}[\Theta_i(\omega)-\Theta_j(\omega)]$. The photon energy $\hbar\omega$ is multiplied to this quantity to obtain the radiation power transfer. Between two reservoirs i and j, there are "direct" terms ($\varepsilon_{1i,1j}$ and $\varepsilon_{2i,2j}$) involving only one of the resonances; "cross" terms ($\varepsilon_{1i,2j}$ and $\varepsilon_{2i,1j}$) involving both resonances. The total transmissivity from reservoir i to j is the sum of them. When the coupling between two resonant modes is zero, i.e. $\kappa=0$, the "cross" terms vanish, and the transmissivity between reservoirs can then be computed by summing over contribution from each mode separately [36].

A few important features of CMT formalism are worth noting. First, in CMT, a resonant mode simply means a well-defined (long-lived) mode which oscillates many cycles before gradually dying out. Mathematically it corresponds to a complex resonant energy whose real part is much larger than the imaginary part. The CMT formalism by itself does not tell the physical origin of the resonant modes, and we have to decide what a resonant mode represents based on our physics understanding. For the single-mode case, the resonant mode is the eigenmode of the *whole* system (including all reservoirs). For the two-mode case, we can choose what the modes are, which will be discussed in the next section. Second, according to CMT, the energy exchange between reservoirs comes from their couplings to common resonant modes. In Eq. (2), the coupling between the resonant mode i and nth loss mechanism (i.e. $\Gamma_{i\,n}$) tends to thermalize the resonant mode according to nth reservoir (if only Γ_{1n} is non-zero, the photon occupation number of the resonant mode is given by Planck distribution at the temperature T_n), and it is the competition between different reservoirs that leads to energy exchange. Finally, there exists an optimal set of parameters that maximize the transmissivity from loss mechanism a to b, which is typically referred to as the "impedance matching" condition [8, 24, 37]. The CMT analysis thus naturally provides a guide on how to enhance the radiation energy transfer in a TPV system [27].

C. Determination of CMT parameters

Now we show how to determine the CMT parameters. In essence, it is done by fitting the CMT resonant energies to those obtained by the system eigen-solver. We first set all source terms $\theta_{+i\,n}$ to zero in Eq. (2). In the ω-space, $\frac{\partial}{\partial t}\to -i\omega$ and we get

$$\begin{aligned}
(\omega-\omega_1+i\sum_n\Gamma_{1n})a_1 &= -\kappa a_2 \\
(\omega-\omega_2+i\sum_n\Gamma_{2n})a_2 &= -\kappa a_1,
\end{aligned} \tag{6}$$

from which the CMT gives the complex eigenenergies of two resonant modes. The obtained resonant energies are then fit to those obtained by the eigen-solver of the whole system. We are interested in the planar structure shown in Fig. 1(a), and the equation to determine the (complex) resonant energies is given in Appendix. The same equation is used to determine the surface plasmon dispersion [38, 39]. For a more complicated structure, an analytical expression may not exist, and some numerical tool, such as finite-difference-time-domain (FDTD) [40], is needed. We find the easiest way to determine $\Gamma_{i\,n}$ is to turn on only loss mechanisms within nth reservoir, and solve for the resonant energies, from which Γ_{1n} and Γ_{2n} can be obtained from their imaginary parts. This will become explicit in the next section where we work out a few examples. As discussed in the previous subsection, the number of resonant modes and what they represent (which affects if some of CMT parameters, such κ and Γ_{ij}, are zero or not) are determined by our physical understanding of the system. Although we only consider two resonant modes here, CMT also works for systems supporting more resonances [41].

III. APPLICATIONS TO SYSTEMS INVOLVING LORENTZIAN DISPERSION

A. Material choice and two elementary configurations

The CMT is successfully applied to the systems involving metal/dielectric interfaces, where surface plasma polariton is the resonant modes [24, 27]. Here we apply the CMT to another class of materials whose dielectric function can be approximated by the Lorentz oscillator model. We fix the Lorentz oscillator model [13] as

$$\epsilon_L(\omega) = \epsilon_\infty \frac{\omega^2 - \omega_{LO}^2 + i\gamma\omega}{\omega^2 - \omega_{TO}^2 + i\gamma\omega}$$

with $\epsilon_\infty = 4.67$. All frequencies are measured in $\omega_{LO} = 0.1616$ eV with $\omega_{TO}/\omega_{LO} = 0.81$, $\gamma/\omega_{LO} = 0.0041$. We also define a $k_{LO} = w_{LO}/c$, and scale all momentums with respect to k_{LO}. ω_{LO} and ω_{TO} are frequencies of longitudinal and transverse optical modes. We also choose an "interband" material, whose dielectric function is governed by the direct interband transition [42, 43].

$$\begin{aligned}
\epsilon_{inter}(\omega) &= \epsilon_r(\omega) + i\epsilon_i(\omega) \\
\epsilon_i(\omega) &= \begin{cases} A\frac{\sqrt{x-1}}{x^2}, & x > 1 \\ 0, & x < 1 \end{cases} \\
\epsilon_r(\omega) &= \begin{cases} B + A\frac{2-\sqrt{1+x}}{x^2}, & x > 1 \\ B + A\frac{2-\sqrt{1+x}-\sqrt{1-x}}{x^2}, & x < 1 \end{cases},
\end{aligned}$$

with $x = \hbar\omega/E_g$. The choice of $(A, B, E_g/\omega_{LO}) = (6, 10, 0.804)$ [13]. In the following, we compute the transmissivity from the bottom Lorentz material to the materials on the top, using both the exact solution and the CMT analysis. Only the TM (transverse magnetic) modes are considered, as the TE (transverse electric) modes have negligible contribution.

We begin by considering the Lorentz-Vacuum-Interband configuration, with the vacuum gap fixed at 10 nm. In this configuration, there is only one resonance originated from the Lorentz material. We compute the transimissivity from Lorentz to interband materials using the exact solution and the CMT procedure. For the exact solution, we compute the Poynting vector $S_z(z = 10\text{ nm})$ using Eq. (1), and identify the $\varepsilon(\omega, k; z = 10\text{ nm})$ as the exact transmissivity. For the CMT including only one resonance and two reservoirs, we have

$$\frac{d}{dt}a_1(t) \to -i\omega a_1 = (-i\omega_1 - \Gamma_{11} - \Gamma_{12})a_1(t) + \sum_{n=1}^{2}\sqrt{2\Gamma_{1n}}\theta_{+1n}.$$

The eigenenergy of CMT is $\omega_1 - i(\Gamma_{11} + \Gamma_{12})$, obtained by the non-zero solution with $\theta_{+1n} = 0$. Once the eigenenergy is obtained from the system eigen-solver, ω_1 is determined by the real part of the resonant energy; Γ_{11} and Γ_{12} are determined by the imaginary part of the resonant energy where the γ in ϵ_L, and imaginary part of ϵ_{inter} is set to zero respectively. Once these parameters are determined, the first line of Eq. (5) is used to compute the transmissivity. As shown in Fig. 2(a) and (c), an almost perfect match between the exact solution and CMT results is seen.

Next we consider the geometry given in Fig. 2(b) – a symmetric Lorentz-Vacuum-Lorentz configuration, with the vacuum gap 10 nm. Following Ref. [24] for the symmetric geometry, we identify a_1 to be the "top" resonant mode, and a_2 to be the bottom resonant mode. Since they are degenerate in energy, we have $\omega_1 = \omega_2 \equiv \omega_0$. Due to the spatially confined distribution of these modes, a_1 mode only couples to the top reservoir, so $\Gamma_{11} \equiv \Gamma$, and $\Gamma_{12} = 0$; a_2 mode only couples to bottom reservoir, so $\Gamma_{22} \equiv \Gamma$, and $\Gamma_{21} = 0$. With this physical understanding, the CMT equations without heat sources are

$$\begin{aligned}
-i\omega a_1 &= (-i\omega_0 - \Gamma)a_1 + i\kappa a_2 \Rightarrow (\omega - \omega_0 + i\Gamma)a_1 = -\kappa a_2 \\
-i\omega a_2 &= (-i\omega_0 - \Gamma)a_2 + i\kappa a_1 \Rightarrow (\omega - \omega_0 + i\Gamma)a_2 = -\kappa a_1
\end{aligned}$$

which have the solutions at $\omega_\pm = \omega_0 - i\Gamma \pm \kappa$. We then find two roots, denoted as $\omega_\pm$ from the system eigen-solver for a given momentum k, and extract the CMT parameters as $\omega_0 = \text{Re}[\omega_+ + \omega_-]/2$, $\kappa = (\omega_+ - \omega_-)/2$, and $\Gamma = \text{Im}\omega_\pm$. The fitted parameters for selected momentum is given in Table I. The second line of Eq. (5) is used to compute the transmissivity. As shown in Fig. 2(b) and (d), a good agreement between exact solution and CMT results is seen.

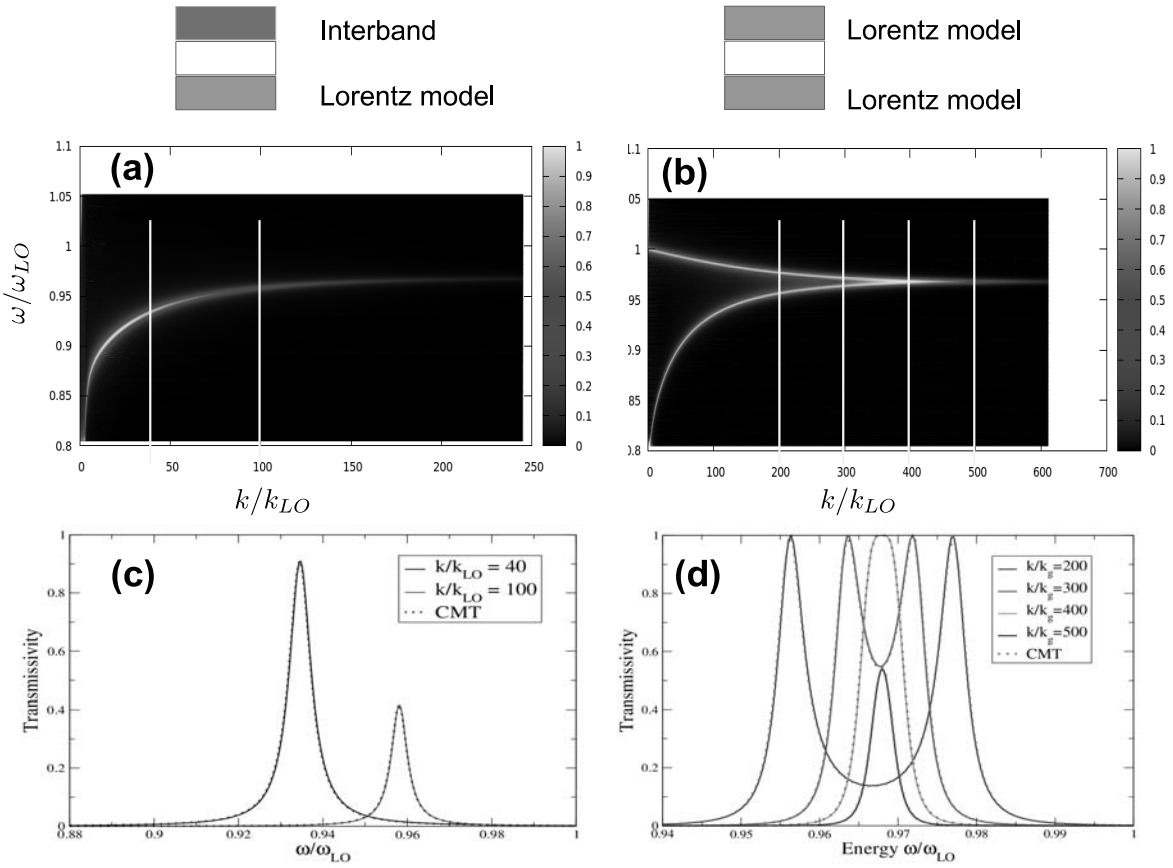

FIG. 2: The exact transimissivity from bottom to top for (a) Lorentz-Vacuum-Interband and (b) Lorentz-Vacuum-Lorentz configurations. For (a), there is only one resonant mode from the Lorentz material; For (b), there are two degenerate resonant modes coming from two Lorentz materials. (c) The transmissivity from bottom Lorentz to top interband material. (d) The transmissivity from bottom to top Lorentz materials as a function of ω for selected momentums, for Lorentz-Vacuum-Lorentz configuration (see Table I). The formalism of two coupled resonant modes is used in the CMT, and an almost perfect agreement is seen.

k/k_{LO}	ω_0	Γ	κ
200	0.156207	0.0003275	0.0017095
300	0.156386	0.0003275	0.0007458
400	0.156420	0.0003275	0.0003290
500	0.156427	0.0003275	0.0001455

TABLE I: The parameters of dielectric-vacuum-dielectricfor selected momentums. ω_0, κ, and Γ are measured in w_{LO}.

B. Asymmetric Lorentz-Vacuum-Lorentz configuration

We now consider an asymmetric Lorentz-Vacuum (10 nm)-Lorentz configuration, where the ω_{LO} and ω_{TO} on the top is 1.01 times larger than those on the bottom. We first *choose* the resonant modes described in the previous subsection: each resonance couples to one of the reservoirs only. The CMT equations without heat sources are

$$\frac{d}{dt}a_1 \to -i\omega a_1 = (-i\omega_1 - \Gamma_1)a_1 - i\kappa a_2$$
$$\frac{d}{dt}a_2 \to -i\omega a_2 = (-i\omega_2 - \Gamma_2)b_2 - i\kappa a_1.$$

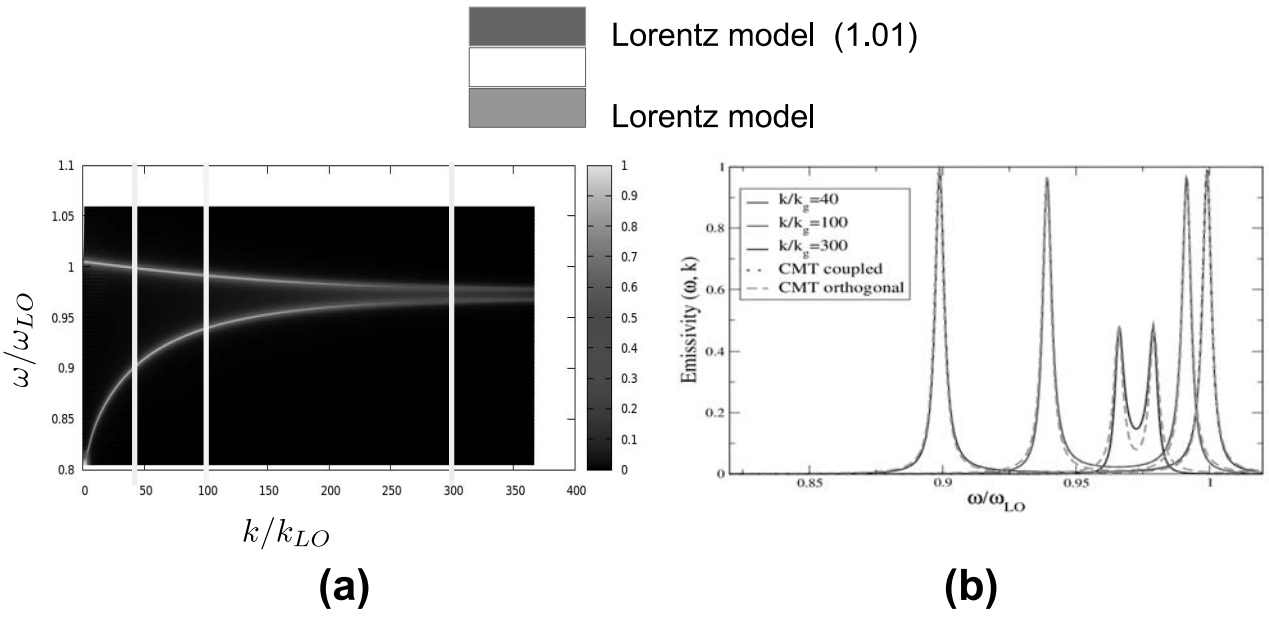

FIG. 3: The emissivity for Lorentz-Vacuum-Lorentz configuration. The bottom $\omega_{LO,b}$ and $\omega_{TO,b}$ are both 1.01 times larger than those of top one. (a) The exact result of $\varepsilon(\omega, k)$. (b) The selected momentum cuts. The CMT with independent modes generally underestimates the emissivity between peaks, but is a good approximation overall. The CMT with coupled modes (see Table II) gives practically the same results.

Here Γ_1 describes the damping of mode a_1 to the 1st reservoir; Γ_2 the damping of a_2 to the 2nd. Writing $\tilde{\omega}_1 = \omega_1 - i\Gamma_1$, $\tilde{\omega}_2 = \omega_2 - i\Gamma_2$, the complex eigenenergies are

$$\begin{aligned}\omega_{\pm}^{(1+2)} &= \frac{\tilde{\omega}_1 + \tilde{\omega}_2}{2} \pm \sqrt{\left(\frac{\tilde{\omega}_1 - \tilde{\omega}_2}{2}\right)^2 + \kappa^2} \\ &= \frac{\omega_1 + \omega_2}{2} - i\frac{\Gamma_1 + \Gamma_2}{2} \pm \sqrt{\left[\frac{\omega_1 - \omega_2}{2} - i\frac{\Gamma_1 - \Gamma_2}{2}\right]^2 + \kappa^2}\end{aligned} \tag{7}$$

The superscript (1+2) means both damping rates to both reservoirs (Γ_1 and Γ_2) are both included. We also compute

$$\begin{aligned}\omega_{\pm}^{(1)} &= \frac{\omega_1 + \omega_2}{2} - i\frac{\Gamma_1}{2} \pm \sqrt{\left[\frac{\omega_1 - \omega_2}{2} - i\frac{\Gamma_1}{2}\right]^2 + \kappa^2} \\ \omega_{\pm}^{(2)} &= \frac{\omega_1 + \omega_2}{2} - i\frac{\Gamma_2}{2} \pm \sqrt{\left[\frac{\omega_1 - \omega_2}{2} + i\frac{\Gamma_2}{2}\right]^2 + \kappa^2} \\ \omega_{\pm}^{(0)} &= \frac{\omega_1 + \omega_2}{2} \pm \sqrt{\left[\frac{\omega_1 - \omega_2}{2}\right]^2 + \kappa^2}\end{aligned} \tag{8}$$

Here $\omega_{\pm}^{(1)}$, $\omega_{\pm}^{(2)}$ are eigenenergies keeping the damping rate to 1st, 2nd reservoir only; $\omega_{\pm}^{(0)}$ are eigenenergies of no damping at all. We go on to express ω_1, ω_2, Γ_1, Γ_2, κ in terms of $\omega_{\pm}^{(i)}$ obtained from the eigen-solver. Denoting

$\bar{\omega}^{(i)} = \frac{1}{2}(\omega_+^{(i)} + \omega_-^{(i)})$ and $\bar{\Delta}^{(i)} = \frac{1}{2}(\omega_+^{(i)} - \omega_-^{(i)})$ to get

$$\begin{aligned}
\frac{\omega_1 + \omega_2}{2} &= \bar{\omega}^{(0)} \\
\Gamma_1 &= 2i(\bar{\omega}^{(1)} - \bar{\omega}^{(0)}) \\
\Gamma_2 &= 2i(\bar{\omega}^{(2)} - \bar{\omega}^{(0)}) \\
\frac{\omega_1 - \omega_2}{2} &= -\frac{[\bar{\Delta}^{(1)}]^2 - [\bar{\Delta}^{(0)}]^2 + \Gamma_1^2/4}{i\Gamma_1} = +\frac{[\bar{\Delta}^{(2)}]^2 - [\bar{\Delta}^{(0)}]^2 + \Gamma_2^2/4}{i\Gamma_2} \\
\kappa^2 &= [\bar{\Delta}^{(0)}]^2 - \left[\frac{\omega_1 - \omega_2}{2}\right]^2
\end{aligned} \tag{9}$$

For the fitting procedure in Eq. (9), we assume that the ω_1, ω_2, and κ stay unchanged when "deactivating" Γ_1 and/or Γ_2, which is approximately true. Typically, the changes of ω_1, ω_2, and κ are less than 0.1%. The CMT parameters for selected momentums are given in Table II. The second line of Eq. (5) is then used to compute the transmissivity. As shown in Fig. 3(a) and (b), a good agreement between the exact solution and CMT results is achieved.

k/k_{LO}	ω_1	ω_2	Γ_1	Γ_2	κ^2
40	0.953660	0.944202	0.0020264	0.0020264	6.529699e-05
100	0.970081	0.960468	0.0020266	0.0020266	1.744244e-05
300	0.977628	0.967946	0.0020266	0.0020266	1.09060e-07

TABLE II: The parameters of dielectric-vacuum-dielectric(1.1) for selected momentums. ω's and Γ's are measured in w_{LO}, κ^2 in w_{LO}^2.

We can also choose two uncoupled resonances for the CMT computation. In this case, the CMT gives

$$\begin{aligned}
\frac{d}{dt}b_1 \to -i\omega b_1 &= (-i\omega_1 - \Gamma_{11} - \Gamma_{12})b_1 \\
\frac{d}{dt}b_2 \to -i\omega b_2 &= (-i\omega_2 - \Gamma_{21} - \Gamma_{22})b_2.
\end{aligned}$$

The two resonant energies are $\omega_1 - i(\Gamma_{11} + \Gamma_{12})$ and $\omega_2 - i(\Gamma_{21} + \Gamma_{22})$. Similar to the case discussed previously, ω_1 and ω_2 are determined from the real part of the resonant energies; Γ_{11} and Γ_{21} are obtained from the imaginary part of $\omega_\pm^{(1)}$, and Γ_{21} and Γ_{22} from the imaginary part of $\omega_\pm^{(2)}$. The sum of the first and fourth lines of Eq. (5) is used to compute the transmissivity. As shown in Fig. 3(a) and (b), it works quite well when $|\omega_1 - \omega_2| \gg \Gamma$, and is still reasonable when $|\omega_1 - \omega_2| \sim \Gamma$.

One key difference between these two choices is emphasized here. The coupled resonances a_1 and a_2 are spatially confined to one of the reservoirs only, and this is the underlying reason why a_1/a_2 decays only to the 1st/2nd reservoir. The uncoupled resonances b_1 and b_2 are, on the other hand, the resonances of the *whole* systems, so all Γ_{11}, Γ_{12}, Γ_{21}, Γ_{22} are non-zero. Note that, we actually use *more physics information* for the coupled resonances, so there are fewer parameters to determine. In the configuration studied here, the choice of coupled resonances turns out to be better, implying that the assumption of coupled resonance captures the key physics. The choice of uncoupled resonances still give reasonably good results, although it generally does not describe the behavior between resonant energies accurately.

C. Three-interface structure

We now investigate systems of three interfaces. We first consider a system of Lorentz-Vacuum-Interband-Lorentz configuration, which contains three interfaces. As shown in Fig. 4, the thickness of the vacuum and the interband material are chosen to be 10 nm. We consider the radiation transfer from the bottom Lorentz material to (i) the combined top interband and Lorentz materials, and (ii) to the interband material only. The exact solution of transmissivity is $\epsilon(\omega, k; z = 10 \text{ nm})$ in case (i); and is $\epsilon(\omega, k; z = 10 \text{ nm}) - \epsilon(\omega, k; z = 20 \text{ nm})$ in case (ii), with $\epsilon(\omega, k; z)$ defined in Eq. (1). We consider two uncoupled resonant modes, and CMT equations without the heat sources are

$$\begin{aligned}
\frac{d}{dt}b_1 \to -i\omega b_1 &= (-i\omega_1 - \Gamma_{11} - \Gamma_{12} - \Gamma_{13})b_1 \\
\frac{d}{dt}b_2 \to -i\omega b_2 &= (-i\omega_2 - \Gamma_{21} - \Gamma_{22} - \Gamma_{23})b_2.
\end{aligned}$$

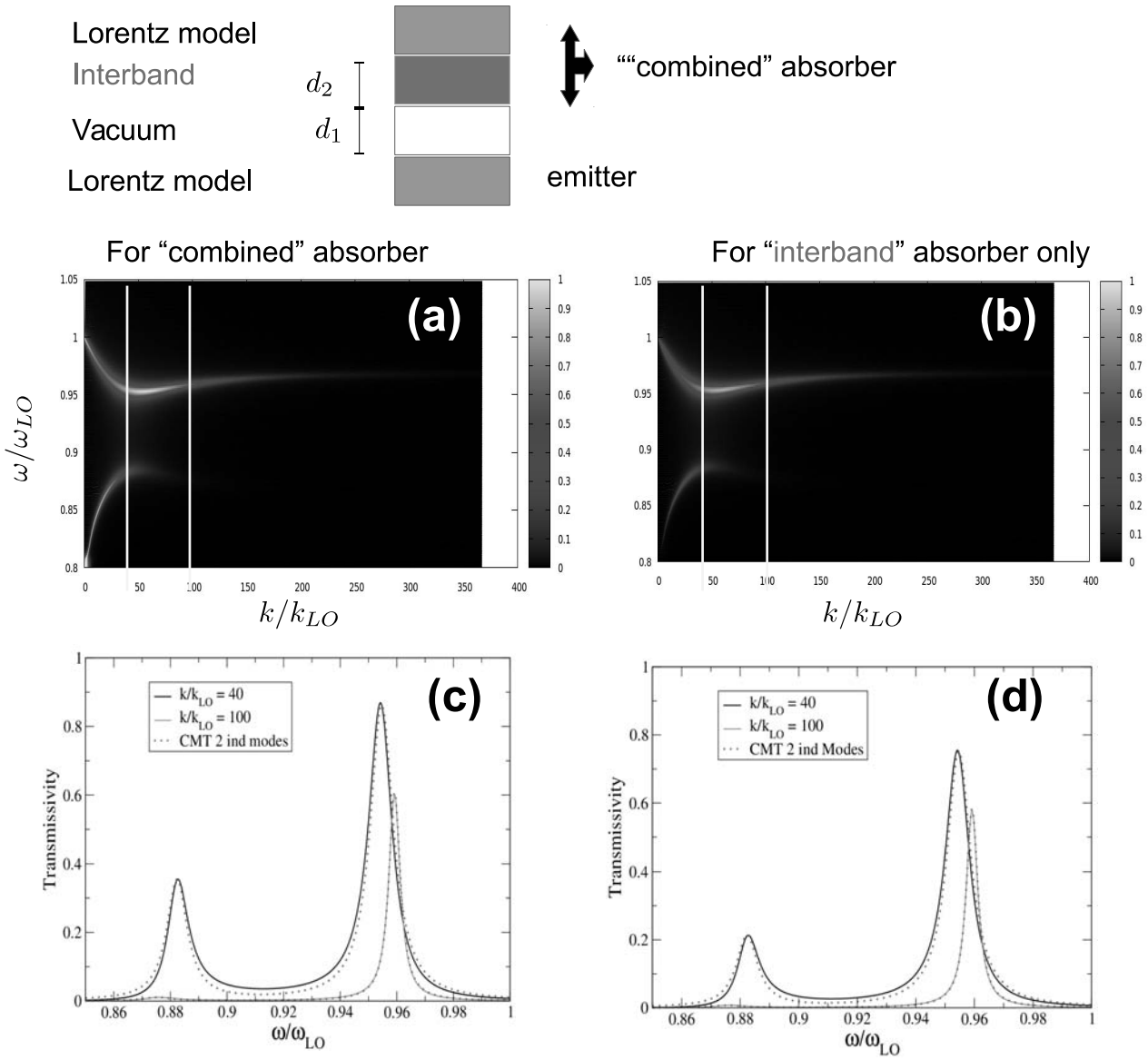

FIG. 4: The exact solution for dielectric-vacuum-interband-dielectric configuration. (a) The exact transmissivity $\varepsilon(\omega, k)$ from bottom Lorentz material to the combined Interband-Lorentz absorber. (b) The exact transmissivity $\varepsilon(\omega, k)$ from bottom Lorentz material to the Interband material only. (c) and (d) The CMT result using two independent resonant modes (see Table III).

The fitting procedure is similar to what we described in the Section III.C, and the CMT parameters of selected momentum are given in Table III. Fig. 4 shows the exact solution and CMT results for both transmissivity, and a reasonably good agreement is again achieved.

As a final example, we consider the Lorentz-Vacuum-Lorentz-Interband configuration, where the thickness of the vacuum and the Lorentz material are chosen to be 10 nm and 4 nm respectively (see Fig. 5). We consider the radiation transfer from the bottom Lorentz material to the interband material, whose exact solution of transmissivity is $\epsilon(\omega, k; z = 14 \text{ nm})$, with $\epsilon(\omega, k; z)$ defined in Eq. (1). We consider two uncoupled resonant modes [Eq. (III C)], and the CMT parameters of selected momentum are given in Table IV. Fig. 5 shows the exact solution and CMT results of the transmissivity, and a reasonably good agreement is observed.

k/k_{LO}	ω_1	ω_2	Γ_{11}	Γ_{12}	Γ_{13}	Γ_{21}	Γ_{22}	Γ_{23}
40	0.95469	0.93009	0.0015666	0.0029925	0.0004394	0.0004285	0.0023994	0.0015894
100	0.95920	0.87544	0.0020068	0.0004422	1.9443e-05	1.6570e-05	0.0046585	0.0020075

TABLE III: The CMT parameters of Lorentz-Vacuum-Interband-Lorentz for selected momentums. ω's and Γ's are measured in w_{LO}.

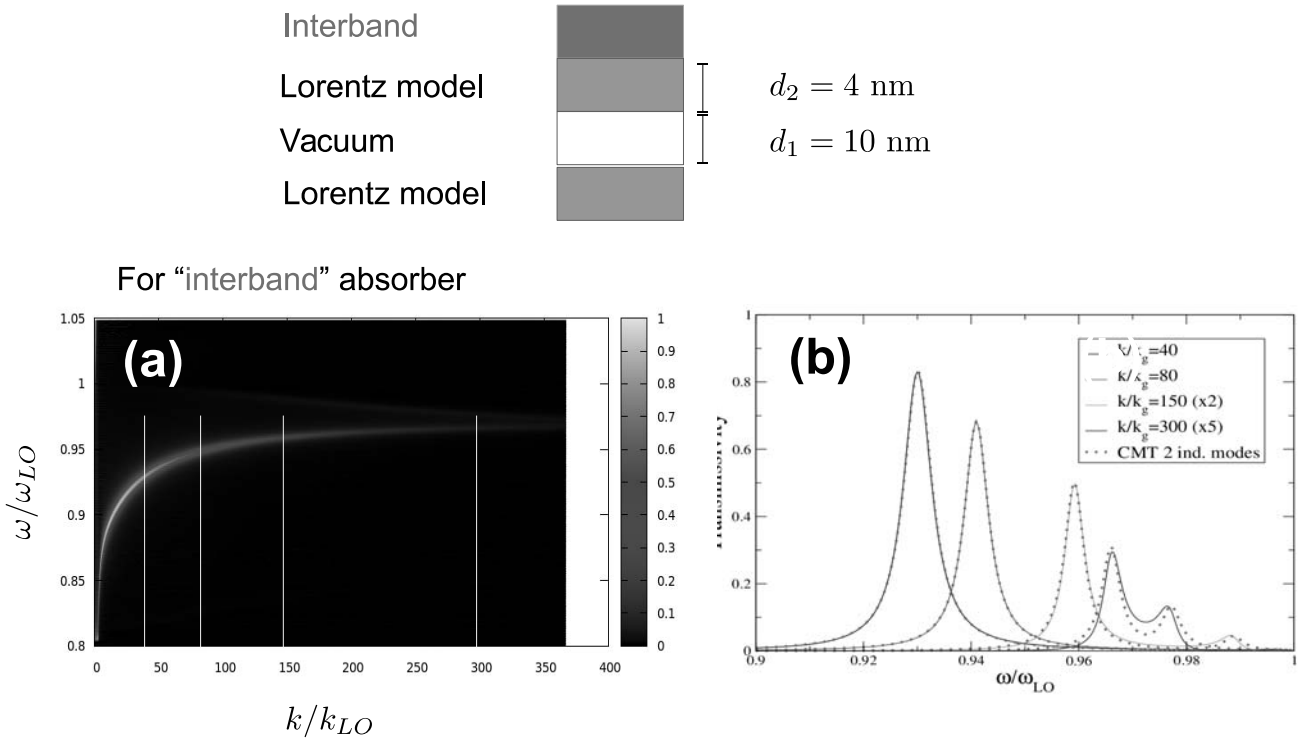

FIG. 5: The exact solution for Lorentz-Vacuum-Interband-Lorentz configuration. (a) The exact $\varepsilon(\omega, k)$ from the bottom Lorentz material to the top interband material. (b) The CMT model based on two independent resonant modes for selected k cuts (see Table IV). The agreement is better when two resonant energies are more separated.

For the structures studied in this subsection, we do not find a model of coupled resonances which gives better results than those of decoupled resonances, therefore only the results of decoupled resonances are shown. Actually, we think the use of decoupled resonances is the big advantage of the CMT analysis, because without prior knowledge of the system, the assumption of two decoupled resonances is the most natural one. A reasonably good agreement to the exact result means that we do not need to know the spatial profile of each resonance to have a good approximated answer.

IV. APPLICATIONS TO ELECTRONIC SYSTEMS

A. Formulation of problem and Landauer's exact expression

The CMT, as it is formulated, does not concern the type of energy carriers. In this section we apply it to the simple electronic systems. The purposes are two-fold. First it demonstrates the generality of CMT analysis. Second, we shall discuss the limitation of CMT, as a numerical solver, in the electronic systems. The configuration of interest is illustrated in Fig. 6 (a) – a left and a right lead which can be regarded as electronic reservoirs characterized by different temperature, chemical potential, and voltage; a small junction, the "scattering region", is coupled to both

k/k_{LO}	ω_1	ω_2	Γ_{11}	Γ_{12}	Γ_{13}	Γ_{21}	Γ_{22}	Γ_{23}
40	0.99863	0.93009	0.0002076	0.0018190	4.3137e-06	0.0018081	0.0002180	0.0011902
80	0.99549	0.94777	0.0003136	0.0017130	2.1284e-05	0.0017070	0.0003196	0.0005160
150	0.98874	0.95917	0.0003670	0.0016595	6.1971e-05	0.0016571	0.0003696	0.0001851
300	0.97718	0.96600	0.0003074	0.0017189	9.0109e-05	0.0017187	0.0003080	3.7831e-05

TABLE IV: The CMT parameters of Lorentz-Vacuum-Lorentz-Interband for selected momentums. ω's and Γ's are measured in w_{LO}.

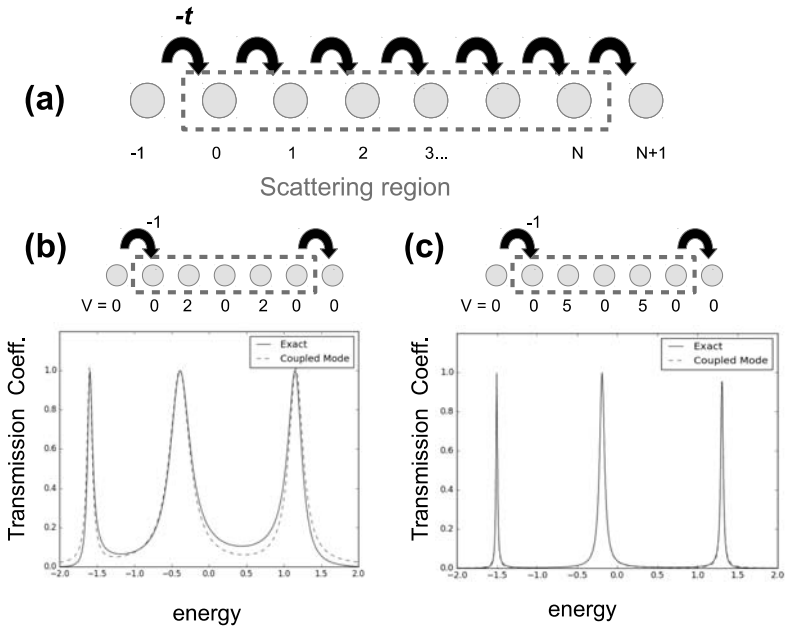

FIG. 6: (a) Schematic representation of electron transport across an arbitrary 1D junction. Sites of $i < 0$ represent a "left" lead; whereas sites of $i > N$ represent a "right" lead. The scattering region represents a junction that provides the electric resistance. (b) and (c) Transmission coefficient comparison between exact and coupled mode theory for four representative cases. The scattering region contains five sites, and the electron hopping amplitude on the left lead, which serves as the energy unit, is fixed as -1. The on-site potential is site-dependent in the scattering region and is given in the figure. The CMT results become closer to the exact Landauer results when the resonances are sharper.

leads. The current across the junction can be expressed

$$I = -e \int dE T(E) \left[n_F(E; T_R, V_R, \mu_R) - n_F(E; T_L, V_L, \mu_L) \right], \tag{10}$$

with the Fermi distribution $n_F(E; T, V, \mu) = \frac{1}{e^{(E-eV-\mu)/T}+1}$. T, V, μ are respectively temperature, voltage, and chemical potential. Like the transmissivity, the transmission coefficient $T(E)$ is *independent of* the thermodynamical parameters T, V, μ of the reservoir, but does depend on the electronic structure of the reservoir. This equation plays the same role as Eq. (1) for the radiative energy transfer.

To proceed, we consider the 5-site scattering region as a concrete example. The goal is to compute the transmission coefficient at a given energy E using Landauer formalism [44]. We outline the computation procedure here. An effective energy-dependent Hamiltonian for this 5-site is defined as

$$\mathbf{H}(E) = \begin{pmatrix} V_0 + \Sigma_L(E) & -t & 0 & 0 & 0 \\ -t & V_1 & -t & 0 & 0 \\ 0 & -t & V_2 & -t & 0 \\ 0 & 0 & -t & V_3 & -t \\ 0 & 0 & 0 & -t & V_4 + \Sigma_R(E) \end{pmatrix} \tag{11}$$

The left/right self energies Σ_L/Σ_R provide all the required information for the coupling between the scattering region and the lead. $-t$ is the hopping within the scattering region, and V_i specifies the on-site potential. We assume the

left and right leads have the tight-binding dispersion

$$E_L(k) = -2t\cos k;\;\; E_R(k) = -2t\cos k.$$

In Eq. (11), the energy-dependent self energies are given by

$$\begin{aligned} \cos(k_L) &= \frac{E}{-2t},\;\; \Sigma_L(E) = -te^{+ik_L a} \\ \cos(k_R) &= \frac{E}{-2t},\;\; \Sigma_R(E) = -te^{+ik_R a}. \end{aligned} \tag{12}$$

By defining $\mathbf{G}(E) = [E - \mathbf{H}(E)]^{-1}$, the retarded and advanced Green's functions are $\mathbf{G}^r(E) = [(E + i\eta) - \mathbf{H}(E)]^{-1}$ and $\mathbf{G}^a(E) = [\mathbf{G}^r(E)]^\dagger$ respectively. The transmission coefficient is by [45, 46]

$$T(E) = 4(\mathrm{Im}\Sigma_R)\left[\mathbf{G}^r\right]_{4,0}(\mathrm{Im}\Sigma_L)\left[\mathbf{G}^a\right]_{0,4} \tag{13}$$

Eq. (13) gives the exact results.

B. CMT results and discussion

Now we give the transmission coefficient using CMT. The CMT needs the complex eigenvalues of $\mathbf{H}(E)$ defined in Eq. (11). We note that because $\mathbf{H}(E)$ has an E dependence, it is not the standard eigenvalue problem. Also, as self energies are generally complex, $\mathbf{H}(E)$ is not a Hermitian and the eigenvalues obtained by $\mathrm{Det}[z_i - \mathbf{H}(z - i)] = 0$ are complex. We denote the eigenvalues as $z_i = E_i + i\Gamma_i$ with i labeled the resonance. To obtain the transmission coefficient, we solve two eigenvalue problems: one which sets $\mathrm{Im}[\Sigma_L] = 0$, and one which sets $\mathrm{Im}[\Sigma_R] = 0$. They are

$$\begin{aligned} z_{i,R} &= E_{i,R} + i\Gamma_{i,R} \;\text{ with } \mathrm{Im}[\Sigma_L] = 0 \\ z_{i,L} &= E_{i,L} + i\Gamma_{i,L} \;\text{ with } \mathrm{Im}[\Sigma_R] = 0 \end{aligned} \tag{14}$$

Generally $E_{i,R} \approx E_{i,L} \equiv E_i$. *Assuming* these resonances do not couple, the transmission coefficient is given by the sum over all resonances as

$$T(E) = \sum_i \frac{4\Gamma_{i,R}\Gamma_{i,L}}{(E - E_i)^2 + (\Gamma_{i,R} + \Gamma_{i,L})^2}. \tag{15}$$

CMT is particularly useful when the resonances are separate in energy. In this case, the transmission coefficient as a function of energy is the sum of Lorentzian profiles [Eq. (15)]. When the real part of the resonant energy *difference* is comparable or even smaller than the imaginary part of the resonance, CMT becomes less useful.

As an example, we consider the case where the scattering region contains five sites, and the electron hopping amplitude on the left lead, which serves us the energy unit, is fixed as -1. Two representative results are given Fig. 6 (b) and (c). In Fig. 6 (b), the on-site potential next to two boundaries are set to +2, whereas In Fig. 6 (c) , they are set to 5. As expected, the CMT results become closer to the exact Landauer results when the resonances are sharper. We have tested many cases, including different left and right leads, or different on-site potentials. Generally, we find if the energy difference is about 10 times (or more) larger than the imaginary part, CMT gives reasonable answers. We emphasize that, by computing the ratio between the energy difference and the imaginary part, a CMT calculation by itself gives an estimate how good the CMT approximation is. Therefore when CMT works, an exact calculation is not needed. Finally, without providing the results, we point out that the above CMT procedure also applies to the phonon energy transfer.

V. CONCLUSION

To conclude, we apply the coupled mode theory to study the radiative heat transfer involving Lorentz materials whose dielectric functions can be approximated by Lorentz oscillator model. Each Lorentz material provides a resonance between ω_{LO} and ω_{TO}, and the CMT gives a generally good approximation for this class of materials. This is established by comparing the transmissivity computed by the exact solution to that computed by CMT. Based on CMT, the heat transfer between reservoirs originates from their couplings to common resonant mode(s). For a system sustaining only one resonance, the resonance represents the a quasi-eigenmode (quasi in the sense of the non-zero

imaginary part) of the whole system. For systems sustaining two resonances, we can choose if the two resonances are coupled or not based on our understanding. Generally, the choice of two decoupled modes is good, especially when two resonances are separated in energy. We regard this as a big advantage of the CMT analysis, in the sense that one does not need to know the spatial distribution of resonance to get a good approximation of radiation energy transfer. However, when the system does not support resonances, CMT analysis is not numerically useful. To demonstrate the generality of CMT analysis, we also apply our CMT procedure to electronic system, where the transmissivity between left and right 1D leads are computed. The similar behavior as the radiative energy transfer is seen. The CMT parameters can be obtained by the complex eigen-solver of the whole system. For the planar structure, the condition of resonances is identical to that used in the surface plasmon calculation. Compared with the exact solution, the CMT provides a simple and clear framework to analyze the radiation energy exchange between reservoirs, and can therefore help the design that aims to maximize the radiative heat transfer from one reservoir to the other.

Acknowledgement

We thank Jian-Jian Wang, Prabhakar Bandaru, and Zhuomin Zhang for helpful discussions.

1. Resonance condition for general layered structures

In the Appendix, we consider the general layered structure: Each layer has its thickness d_i, and we define $\bar{d}_i = \sum_{n=1}^{i} d_n$ (and $\bar{d}_0 \equiv 0$), so the material of ϵ_i ranges from $z = \bar{d}_{i-1}$ to $z = \bar{d}_i$. At $z = \bar{d}_i$, the boundary condition needs to be considered. The general solution of a TM mode is

$$F(z) = \begin{cases} A_0 e^{+K_0 z}, & z < 0 \\ A_{1,+} e^{K_1 z} + A_{1,-} e^{-K_1 z} & 0 < z < d_1 \\ A_{2,+} e^{K_2 z} + A_{2,-} e^{-K_2 z} & \bar{d}_1 < z < \bar{d}_2 \\ ..... & \\ A_{n,+} e^{K_n z} + A_{n,-} e^{-K_n z} & \bar{d}_{n-1} < z < \bar{d}_n \end{cases} \tag{16}$$

where $A_i = \epsilon_i E_z$ (the electric displacement field along z) and $k_x^2 - K_i^2 = \epsilon_i(\omega)(\omega/c)^2$. We define $\gamma_i = K_i/\epsilon_i$ and $y_i \equiv \frac{\gamma_i}{\gamma_{i+1}}$. At the interface $z = \bar{d}_i$, the continuity of $\mathbf{E}_\parallel$ and $\mathbf{H}_\parallel$ (or $F(z)$) lead to [39]

$$\begin{bmatrix} A_{i+1,+} \\ A_{i+1,-} \end{bmatrix} = \hat{X}_i \begin{bmatrix} A_{i,+} \\ A_{i,-} \end{bmatrix} = \begin{bmatrix} e^{-K_{i+1}\bar{d}_i} & 0 \\ 0 & e^{+K_{i+1}\bar{d}_i} \end{bmatrix} \begin{bmatrix} \frac{1}{2}(1+y_i) & \frac{1}{2}(1-y_i) \\ \frac{1}{2}(1-y_i) & \frac{1}{2}(1+y_i) \end{bmatrix} \begin{bmatrix} e^{+K_i\bar{d}_i} & 0 \\ 0 & e^{-K_i\bar{d}_i} \end{bmatrix} \begin{bmatrix} A_{i,+} \\ A_{i,-} \end{bmatrix}. \tag{17}$$

For an n-interface configuration ($n+1$ materials specified by ϵ_0, ϵ_1, ... to ϵ_n), we get

$$\begin{bmatrix} A_{n,+} \\ A_{n,-} \end{bmatrix} = \hat{X}_{n-1} \cdots \hat{X}_2 \hat{X}_1 \hat{X}_0 \begin{bmatrix} A_{0,+} \\ A_{0,-} \end{bmatrix} \equiv \begin{bmatrix} Y_{11} & Y_{12} \\ Y_{21} & Y_{22} \end{bmatrix} \begin{bmatrix} A_{0,+} \\ A_{0,-} \end{bmatrix} \tag{18}$$

For a bounded solution, $A_{0-} = A_{n+} = 0$, i.e.

$$\begin{bmatrix} 0 \\ A_{n,-} \end{bmatrix} = \begin{bmatrix} Y_{11} & Y_{12} \\ Y_{21} & Y_{22} \end{bmatrix} \begin{bmatrix} A_{0,+} \\ 0 \end{bmatrix}.$$

Therefore the condition of eigenmodes are $Y_{11} = 0$ in this case. For the three-interface (four materials) configuration, by defining $e_1 = e^{K_1 d_1}$ and $e_2 = e^{K_2 d_2}$, we have

$$\begin{aligned} Y_{11} \propto\ & (1+y_2)(1+y_1)(1+y_0)e_2 e_1 + (1+y_2)(1-y_1)(1-y_0)e_2 e_1^{-1} \\ & + (1-y_2)(1-y_1)(1+y_0)e_2^{-1} e_1 + (1-y_2)(1+y_1)(1-y_0)e_2^{-1} e_1^{-1}. \end{aligned} \tag{19}$$

The roots gives the resonant energies. If $\epsilon_2 = \epsilon_3$, $y_2 = 1$ and

$$Y_{11} \propto 2e_2[(1+y_1)(1+y_0)e_1 + (1-y_1)(1-y_0)e_1^{-1}]. \tag{20}$$

The condition $(1+y_1)(1+y_0)e_1 + (1-y_1)(1-y_0)e_1^{-1} = 0$ gives the resonant energies for any two-interface configurations. Finally if $\epsilon_1 = \epsilon_2$, $y_1 = 1$ and $1 + y_0 = 0$ gives the resonant energies for any one-interface configurations.

[1] H. A. Haus and W. Huang, Proceedings of the IEEE **79**, 1505 (1991), ISSN 0018-9219.

[2] A. W. Snyder, J. Opt. Soc. Am. **62**, 1267 (1972), URL http://www.osapublishing.org/abstract.cfm?URI=josa-62-11-1267.

[3] W.-P. Huang, J. Opt. Soc. Am. A **11**, 963 (1994), URL http://josaa.osa.org/abstract.cfm?URI=josaa-11-3-963.

[4] S. Fan, W. Suh, and J. D. Joannopoulos, J. Opt. Soc. Am. A **20**, 569 (2003), URL http://josaa.osa.org/abstract.cfm?URI=josaa-20-3-569.

[5] A. Kurs, A. Karalis, R. Moffatt, J. D. Joannopoulos, P. Fisher, and M. Soljačić, Science **317**, 83 (2007), ISSN 0036-8075, http://science.sciencemag.org/content/317/5834/83.full.pdf, URL http://science.sciencemag.org/content/317/5834/83.

[6] B. L. Cannon, J. F. Hoburg, D. D. Stancil, and S. C. Goldstein, IEEE Transactions on Power Electronics **24**, 1819 (2009), ISSN 0885-8993.

[7] H. Chalabi, E. Hasman, and M. L. Brongersma, Opt. Express **22**, 30032 (2014), URL http://www.opticsexpress.org/abstract.cfm?URI=oe-22-24-30032.

[8] L. Zhu, S. Sandhu, C. Otey, S. Fan, M. B. Sinclair, and T. Shan Luk, Applied Physics Letters **102**, 103104 (2013), URL http://scitation.aip.org/content/aip/journal/apl/102/10/10.1063/1.4794981.

[9] P. Davies and A. Luque, Solar Energy Materials and Solar Cells **33**, 11 (1994), ISSN 0927-0248, URL http://www.sciencedirect.com/science/article/pii/0927024894902844.

[10] R. S. DiMatteo, P. Greiff, S. L. Finberg, K. A. Young-Waithe, H. K. H. Choy, M. M. Masaki, and C. G. Fonstad, Applied Physics Letters **79**, 1894 (2001), http://dx.doi.org/10.1063/1.1400762, URL http://dx.doi.org/10.1063/1.1400762.

[11] M. D. Whale and E. G. Gravaiho, IEEE Power Engineering Review **22**, 67 (2002), ISSN 0272-1724.

[12] N.-P. Harder and P. Wrfel, Semiconductor Science and Technology **18**, S151 (2003), URL http://stacks.iop.org/0268-1242/18/i=5/a=303.

[13] A. Narayanaswamy and G. Chen, Applied Physics Letters **82** (2003).

[14] P. Bermel, M. Ghebrebrhan, W. Chan, Y. X. Yeng, M. Araghchini, R. Hamam, C. H. Marton, K. F. Jensen, M. Soljačić, J. D. Joannopoulos, et al., Opt. Express **18**, A314 (2010), URL http://www.opticsexpress.org/abstract.cfm?URI=oe-18-103-A314.

[15] A. Lenert, D. M. Bierman, Y. Nam, W. R. Chan, I. Celanović, M. Soljacic, and E. N. Wang, Nat Nano **9**, 126 (2014), URL http://dx.doi.org/10.1038/nnano.2013.286.

[16] D. M. Bierman, A. Lenert, W. R. Chan, B. Bhatia, I. Celanović, M. Soljacic, and E. N. Wang, Nature Energy **1**, 16068 (2016), URL http://dx.doi.org/10.1038/nenergy.2016.68.

[17] S. Basu and Z. M. Zhang, Appl. Phys. Lett. **95**, 133104 (2009).

[18] T. J. Bright, L. P. Wang, and Z. M. Zhang, Journal of Heat Transfer **136**, 062701 (2014).

[19] S. M. Rytov, Y. A. Kravtsov, and V. I. Tatarski, *Principles of Statistical Radiophysics, Vol. 3.* (Springer, Berlin, 1987).

[20] D. Polder and M. Van Hove, Phys. Rev. B **4**, 3303 (1971), URL http://link.aps.org/doi/10.1103/PhysRevB.4.3303.

[21] A. A. Maradudin and D. L. Mills, Phys. Rev. B **11**, 1392 (1975), URL http://link.aps.org/doi/10.1103/PhysRevB.11.1392.

[22] K. Joulain, J.-P. Mulet, F. Marquier, R. Carminati, and J.-J. Greffet, Surface Science Reports **57**, 59 (2005), ISSN 0167-5729, URL http://www.sciencedirect.com/science/article/pii/S0167572905000105.

[23] H. B. Callen and T. A. Welton, Phys. Rev. **83**, 34 (1951), URL http://link.aps.org/doi/10.1103/PhysRev.83.34.

[24] A. Karalis and J. D. Joannopoulos, Applied Physics Letters **107**, 141108 (2015), URL http://scitation.aip.org/content/aip/journal/apl/107/14/10.1063/1.4932520.

[25] P. Wurfel, Journal of Physics C: Solid State Physics **15**, 3967 (1982), URL http://stacks.iop.org/0022-3719/15/i=18/a=012.

[26] P. Würfel, S. Finkbeiner, and E. Daub, Applied Physics A **60**, 67 (1995), ISSN 1432-0630, URL http://dx.doi.org/10.1007/BF01577615.

[27] A. Karalis and J. D. Joannopoulos, Scientific Reports **6**, 141108 (2016), URL http://dx.doi.org/10.1038/srep28472.

[28] W. G. Spitzer, D. Kleinman, and D. Walsh, Phys. Rev. **113**, 127 (1959), URL http://link.aps.org/doi/10.1103/PhysRev.113.127.

[29] M. I. Eremets, M. Gauthier, A. Polian, J. C. Chervin, J. M. Besson, G. A. Dubitskii, and Y. Y. Semenova, Phys. Rev. B **52**, 8854 (1995), URL http://link.aps.org/doi/10.1103/PhysRevB.52.8854.

[30] C. T. Chen and B. D. Cahan, J. Opt. Soc. Am. **71**, 932 (1981), URL http://www.osapublishing.org/abstract.cfm?URI=josa-71-8-932.

[31] L. Genzel, T. P. Martin, and U. Kreibig, Zeitschrift für Physik B Condensed Matter **21**, 339 (1975), ISSN 1431-584X, URL http://dx.doi.org/10.1007/BF01325393.

[32] R. S. DiMatteo, P. Greiff, S. L. Finberg, K. A. YoungWaithe, H. K. H. Choy, M. M. Masaki, and C. G. Fonstad, AIP Conference Proceedings **653** (2003).

[33] R. DiMatteo, P. Greiff, D. Seltzer, D. Meulenberg, E. Brown, E. Carlen, K. Kaiser, S. Finberg, H. Nguyen, J. Azarkevich, et al., AIP Conference Proceedings **738** (2004).

[34] S.-A. Biehs, M. Tschikin, and P. Ben-Abdallah, Phys. Rev. Lett. **109**, 104301 (2012), URL https://link.aps.org/doi/10.1103/PhysRevLett.109.104301.

[35] The second and fourth lines of Eq. (2) is different from Eq.(1) and Eq.(8) in Ref. [24] by a minus sign. This convention does not change any physical observables.

[36] Note that for the planar configuration, resonances of different in-plane momentum **K** do not couple due to symmetry argument, and therefore the total emissivity involves an integral over all momentums.

[37] C. Lin, B. Wang, K. H. Teo, and P. Bandaru, Phys. Rev. Applied **7**, 034003 (2017), URL https://link.aps.org/doi/

10.1103/PhysRevApplied.7.034003.
[38] E. N. Economou, Phys. Rev. **182**, 539 (1969), URL http://link.aps.org/doi/10.1103/PhysRev.182.539.
[39] E. N. Economou and K. L. Ngai, *Surface Plasma Oscillations and Related Surface Effects in Solids* (John Wiley & Sons, Inc., 2007), pp. 265–354, ISBN 9780470143797, URL http://dx.doi.org/10.1002/9780470143797.ch3.
[40] A. Taflove, A. Oskooi, and S. G. Johnson, eds., *Advances in FDTD Computational Electrodynamics: Photonics and Nanotechnology* (Norwood, MA: Artech House, 2013).
[41] H. Iizuka and S. Fan, Journal of Applied Physics **120**, 194301 (2016), http://dx.doi.org/10.1063/1.4967832, URL http://dx.doi.org/10.1063/1.4967832.
[42] D. E. Aspnes and A. A. Studna, Phys. Rev. B **27**, 985 (1983), URL http://link.aps.org/doi/10.1103/PhysRevB.27.985.
[43] S. Adachi, Phys. Rev. B **35**, 7454 (1987), URL http://link.aps.org/doi/10.1103/PhysRevB.35.7454.
[44] R. Landauer, IBM Journal of Research and Development **1** (1957).
[45] Y. Meir, N. S. Wingreen, and P. A. Lee, Phys. Rev. Lett. **66**, 3048 (1991), URL http://link.aps.org/doi/10.1103/PhysRevLett.66.3048.
[46] Y. Meir, N. S. Wingreen, and P. A. Lee, Phys. Rev. Lett. **70**, 2601 (1993), URL http://link.aps.org/doi/10.1103/PhysRevLett.70.2601.